

# Development of an Anthropomorphic Breast Software Phantom Based on Region Growing Algorithm

Cuiping Zhang, Predrag R. Bakic, Andrew D.A. Maidment

Department of Radiology, University of Pennsylvania,  
3400 Spruce Street, Philadelphia, PA 19104

Cuiping.Zhang | Predrag.Bakic | Andrew.Maidment@uphs.upenn.edu

## ABSTRACT

Software breast phantoms offer greater flexibility in generating synthetic breast images compared to physical phantoms. The realism of such generated synthetic images depends on the method for simulating the three-dimensional breast anatomical structures. We present here a novel algorithm for computer simulation of breast anatomy. The algorithm simulates the skin, regions of predominantly adipose tissue and fibro-glandular tissue, and the matrix of adipose tissue compartments and Cooper's ligaments. The simulation approach is based upon a region growing procedure; adipose compartments are grown from a selected set of seed points with different orientation and growth rate. The simulated adipose compartments vary in shape and size similarly to the anatomical breast variation, resulting in much improved phantom realism compared to our previous simulation based on geometric primitives. The proposed simulation also has an improved control over the breast size and glandularity. Our software breast phantom has been used in a number of applications, including breast tomosynthesis and texture analysis optimization.

**Keywords:** Modeling, Visualization, Breast Phantom, Validation, Simulation of breast image acquisition.

## 1. INTRODUCTION

Breast phantoms have been used as test objects for a number of applications in clinical breast imaging including quality assessment in mammography<sup>1</sup>, optimization of imaging modalities<sup>2</sup>, and evaluation of image post-processing algorithms<sup>3</sup>. Common physical phantoms are made using uniform material (e.g., Lucite) which can mimic X-ray attenuation in breast tissues. These phantoms do not simulate parenchymal patterns, the complex mammographic background generated by projection of breast anatomical structures. Parenchymal patterns, in the form of anatomical noise<sup>4,5</sup>, may affect the visibility of breast lesions. Some breast phantoms are designed to mimic the appearance of a unique breast clinical image (e.g., an anthropomorphic mammography phantom<sup>6</sup>); however, they cannot simulate the population variation in breast anatomy.

Computer simulated phantoms provide a flexible alternative to physical models, offering the possibility to generate very complex, subtle anatomical variations. There are two-dimensional (2D) breast models that can be used to generate synthetic images with matching statistical properties of clinical images<sup>7,8</sup>. However, those models cannot provide realistic three-dimensional (3D) rendering of the underlying parenchymal patterns. Only 3D simulation of the breast anatomy can provide insight into the formation of parenchymal patterns.

There have been several efforts to design realistic software breast phantoms. Taylor et al<sup>9</sup> simulated the growth of duct systems within a breast volume. Bliznakova et al<sup>10</sup> introduced a hybrid method that simulates normal breast tissue structures and abnormalities, using geometric primitives and an approximation of the anatomical noise estimated from clinical images. Bakic et al<sup>11,12</sup> proposed a 3D anthropomorphic computer breast phantom, based on the simulation of breast anatomical structures, a model of breast deformation during mammographic compression, and an X-ray image acquisition model; such an approach was used to generate synthetic parenchymal pattern with similar texture properties to clinical mammograms<sup>5,13-15</sup>.

We present here a novel algorithm for computer simulation of breast anatomy as an extension of the Bakic phantom. We generated the breast outline and the large scale tissue regions using an approach similar to Bakic. The internal adipose compartments were simulated using a seeded region-growing algorithm, starting from a randomly selected set of seed

points. The region growing algorithm provides more compact volume coverage and more realistic appearance of the synthetic mammograms compared to the simulation based on spherical approximation of adipose compartments, originally used by Bakic

## 2. MATERIALS AND METHODS

### 2.1 Breast anatomy and its appearance in clinical X-ray images

The major types of breast tissue, distinguishable both in histological slides and clinical X-ray images are fibro-glandular tissue (FGT), and adipose tissue (AT)<sup>16</sup>. Fibro-glandular tissue refers to a combination of the glandular, parenchymal tissue, and the fibrous connective, stromal tissue physically supporting the breast. Adipose tissue is organized into groups of fatty cells, forming macroscopically visible adipose compartments, surrounded by connective tissue. Extensions of the connective tissue that are attached to the skin for breast support are called the Cooper's ligaments.<sup>17</sup> The breast gland is positioned between the superficial and deep layers of the fascia mammae. The superficial fascia layer is separated from the skin by 0.5-2.5 cm thick layer of subcutaneous fat; the deeper fascia layer is separated from the pectoralis major by a layer of retromammary fat<sup>17</sup>.

Overall, the breast consists of a predominantly FGT region, surrounded by a predominantly AT region, as seen in a subgross histologic slide, Figure 1(a). Histologic slides only show the 2D spatial relationship of various breast tissues; their 3D relationship is illustrated in drawings of the breast anatomical preparations made by Sir A. P. Cooper<sup>17</sup>(Fig. 1(b)). The adipose tissue was removed during the preparation of anatomical samples.



**Figure 1:** (a) Subgross (thick) histologic slide showing a predominantly FGT region surrounded by a predominantly AT region. (courtesy of R.D. Cardiff) (b) A section of the mammary gland.

In clinical X-ray images, breast anatomy is visualized based on X-ray attenuation differences between various tissue types. With the X-ray energy normally used in breast imaging, fibrous and glandular tissue structures have practically the same X-ray attenuation coefficient; the attenuation coefficient for the adipose tissue is about half of the attenuation for fibro-glandular tissue<sup>18</sup>. Fig. 2(a) shows a coronal breast CT of a mastectomy specimen<sup>19</sup>, and Fig. 2(b) shows a clinical mammographic image. Adipose compartments and the Cooper's ligaments are visible in both images; they are more easily distinguishable in the CT image. Projections of the adipose compartments and the connective tissue structures in the breast form the characteristic parenchymal pattern seen in clinical X-ray images of the breast.

Our breast phantom simulates the skin, large scale regions of AT and FGT, the matrix of Cooper's ligaments and adipose tissue compartments. The version of the phantom presented here does not model the ducts explicitly; we included a simulated ductal network in our previous version of the phantom<sup>20</sup>. The predominantly AT region has compact coverage of adipose compartments of different size, while the predominantly FGT region has fewer, more separated compartments, as seen in Fig. 2(a).

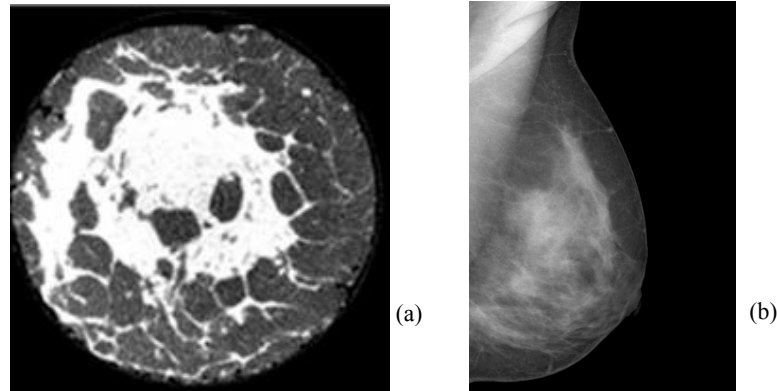


**Figure 2:** (a) A breast CT slice of a mastectomy specimen (courtesy of S. Glick). (b) A clinical mammogram.

## 2.2 Simulation of predominantly AT and FGT regions

We start with the design of our software breast phantom assuming the breast is positioned to a mammographic medio-lateral oblique (MLO) view. The sagittal plane is defined to be parallel with the MLO plane; the phantom outline is symmetric about the center sagittal plane; the current version of the phantom does not include the pectoral muscle. The MLO view is also used in digital breast tomosynthesis. We modeled two large-scale breast tissue regions: the FGT region and the surrounding AT region. The sagittal symmetry plane of the model corresponds to the MLO view plane, as shown in Fig. 3(a).

The breast outline is approximated by two ellipsoidal surfaces, attached transversely at the nipple level, as seen in Fig. 3(b). The breast phantom is covered by a thin layer simulating skin. Fig. 3 shows orthogonal cross sections of a simple breast phantom with only large scale structures. Without further simulation of middle scale elements, the FGT region is considered to be purely fibro-glandular while the AT region is purely fatty.

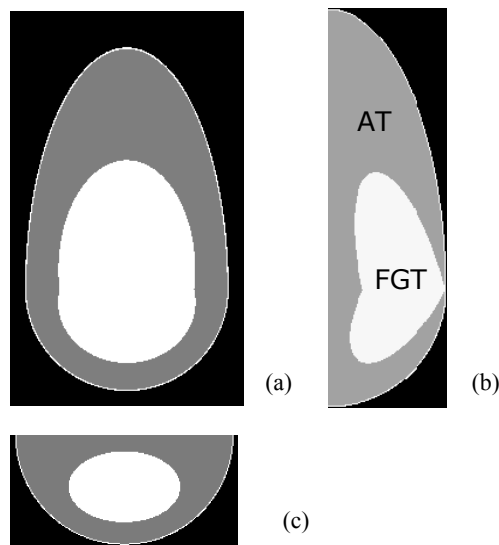


**Figure 3:** Three orthogonal slices of a phantom that includes only the skin, the large scale structures: the FGT and the AT regions. (a) Coronal view. (b) Sagittal view. (c) Transverse view.

The size and the shape of the software breast phantom outline, and the size, shape, and position of the FGT region can be interactively specified during the simulation. A customized user interface was developed to allow selection of different modeling parameters and display simulation results.

Breast density is a known independent factor of breast cancer risk.<sup>21</sup> It is typically measured mammographically as the percent density (PD), the percentage of breast area occupied by the dense, non-fatty tissue (i.e., the skin, the fibrous and

glandular tissues). For our 3D software breast phantom, we use a volumetric, 3D percent density, defined as the percentage of the phantom volume occupied by the simulated dense tissue.

### 2.3 Region growing-based algorithm for modeling Cooper’s ligaments and adipose compartments

Breast adipose compartments, as visualized by subgross histology images, mastectomy specimen radiographs, and clinical mammograms, appear to have irregular shape, varying size, and non-uniform distribution throughout the breast. The adipose cavities inside the FGT region are relatively small and scattered among fibro-glandular tissue structures, while the adipose compartments inside the AT region are densely packed, separated by the fibrous walls and Cooper’s ligaments, and bounded by the skin and the border between the AT and FGT regions.

In this paper we proposed a region growing simulation of adipose compartments and Cooper’s ligaments in our software breast phantom. In medical image analysis, region growing algorithms have usually been applied for image segmentation based on region homogeneity<sup>22, 23</sup>. In our project, region growing is used for a realistic, simultaneous simulation of the large number of adipose compartments, providing variability in their shape, size, and distribution. The simulation is initialized by a selection of seed pixels. A region is grown from each seed, assuming an ellipsoidal shape and selected orientation and growth rate. This growth continues until the neighboring compartments touch each other, after which the boundary pixels in contact become inactive. With the continuation of this growing procedure, the initial ellipsoidal compartment shape is gradually transformed into a more realistic, irregular one. Adipose compartments in the AT region are simulated first, followed by the simulation of cavities inside the FGT region; this approach provides more control over the glandularity of the software phantom.

#### 2.2.1 Initialization of the region growing procedure

The number of compartment seeds can be roughly estimated based on clinical images or histological slides. We measured approximate compartment volumes and compared them with the total breast volume. In mastectomy specimen breast CT images<sup>19</sup> (see Fig. 2(a)), we estimated around 200 compartments. The seeds are randomly selected with slightly denser distribution near the nipple, resulting in relatively smaller compartments in the retroareolar area. The growth rate of each compartment is randomly set. Each compartment grows with an initial shape approximated by an ellipsoid. Orientation of ellipsoids is selected randomly with several constraints described in Fig. 4: The compartments are positioned approximately radial to the nipple–chest wall midline, and fan out from the nipple to the chest wall. Such an initial orientation scheme is used to provide a realistic appearance of the compartments at the end of the region growing procedure.

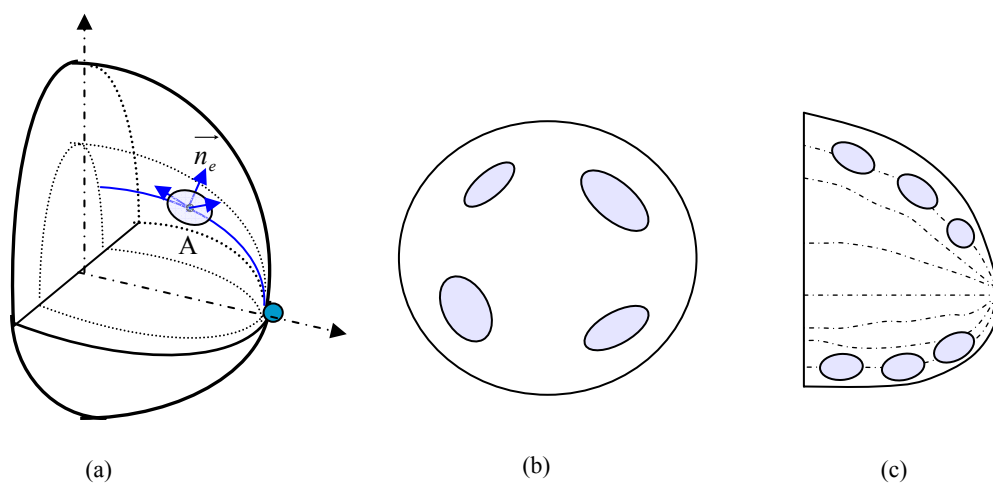


**Figure 4:** Illustration of the compartment orientation scheme at the initialization of the region growing procedure. (a) The compartment seeded at point A is oriented so that its shortest axis corresponds to the surface normal of an ellipsoid passing through the nipple and the seed point A. (b) A coronal section of the phantom illustrating distribution of compartments approximately radial to the nipple–chest wall midline. (c) The compartments fan out from the nipple to the chest wall, as seen in this sagittal section through the nipple.

### 2.3.2 Region growing procedure

Different region growing rates are implemented with the help of a virtual clock in an iterative procedure. The virtual clock's time unit is determined by the fastest growing compartment. Each compartment is updated after a certain number of time units, depending on the compartment's growth rate. A unique table is created for each compartment to keep track of all its active boundary points in the dynamic growing simulation. A table initially contains only the seed point of the corresponding compartment. During the iterative procedure, a compartment expands ellipsoidally and its associated table is updated iteratively to record the active boundary points and discard points that become internal or inactive in the growing process; the inactive points are stored in a separate table used for postprocessing (see Section 2.4). A boundary point becomes inactive once it detects another object in its neighborhood. An inactive boundary point prevents the compartment from expanding at this point. When there are no more active points in a table, the compartment has grown to full contact with its neighboring compartments. Fig. 5 shows the pseudo code for the iterative region growing procedure.

```
Step 1: Set initial parameters
Step 2: Iterative growing procedure
    clock = 0
    While stopping criteria are not met
        {
            clock = clock + 1
            For all compartments, repeat:
                {
                    If the  $i^{\text{th}}$  compartment is active and it needs updating
                        {
                            Calculate current ellipsoid parameters
                            Call subroutine to update this compartment
                        }
                }
        }
Step 3: Show simulated phantom and statistical results
```

**Figure 5:** Pseudo code for the region growing procedure.

Two different stopping criteria are used to simulate different distributions of compartments in the AT and FGT regions. In the AT region, all compartments grow until they are in full contact with their neighboring compartments, the skin, or the AT/FGT border. The AT region compartments may grow beyond the AT/FGT region border, up to individually selected distances, to provide for a less geometric appearance of the AT/FGT border in the synthetic images

As visualized in clinical images and histologic slides, the adipose compartments in the FGT region are smaller and less compact compared to the AT region compartments. This compartment distribution can be simulated by stopping the region growing simulation while all or most of the compartments are still active. During the FGT region growing procedure, we track the volumetric PD of the software phantom, and stop the growing when a desired PD value is obtained.

### 2.4 Postprocessing of simulated compartment walls and imaging acquisition model

The average thickness of the adipose compartment walls, at the end of the region growing procedure, is 3 voxels. In order to have more control over the thickness, we applied a postprocessing step to the compartment walls following the region growing simulation. The postprocessing includes 3D thinning and dilation<sup>24</sup>. The compartment walls are first thinned to one voxel thickness, based on the analysis of the tables of inactive points generated during the region growing procedure. This step is followed by a 3D morphological dilation operation, which is applied iteratively until the desired physical thickness of compartment walls is met. Synthetic images generated with different thickness of compartment walls are shown in Figure 11.

The described region growing procedure was implemented using MATLAB (version 7.3, The MathWorks, Inc. Natick, MA). A customized user interface was developed to allow selection of different modeling parameters and display simulation results. The phantoms shown in this paper were generated with spatial resolution of 200 or 500 $\mu\text{m}/\text{voxel}$ . To

visualize the effects of different simulation parameters on phantom images, we generated synthetic X-ray projections of the uncompressed phantom assuming a monoenergetic, parallel beam X-ray acquisition model. The linear X-ray attenuation coefficients were selected as  $\mu_1 = 0.456 \text{ cm}^{-1}$  for adipose tissue and  $\mu_2 = 0.802 \text{ cm}^{-1}$  for glandular and connective tissue and skin at 20keV<sup>18,25</sup>. An accompanying paper<sup>26</sup> presents the use of our phantoms in simulation of digital breast tomosynthesis; a finite element model is used to simulate the physical breast deformation and a perspective projection model is assumed.

### 3 RESULTS

We have analyzed the synthetic images of the phantoms with varying cup size, percent density, compartment size, and compartment wall thicknesses. Fig. 6 shows three orthogonal slices and a simulated X-ray projection through a software breast phantom. In the phantom sections, the tissue distribution is visualized using the look-up table of unique gray values assigned to each tissue type.

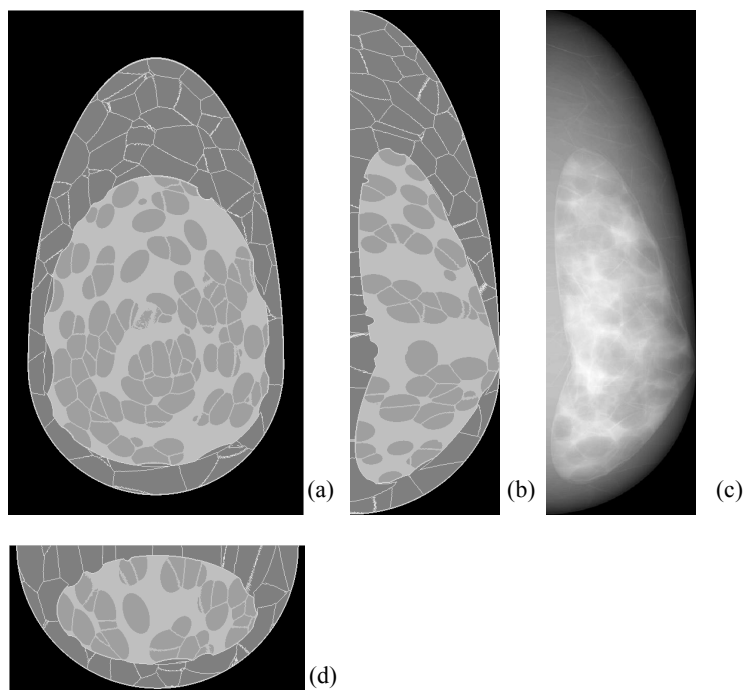


**Figure 6:** Three orthogonal sections of a software breast phantom: (a) Coronal section; (b) Central sagittal section (corresponding to mammographic MLO view); (c) Transverse section, and (d) a simulated X-ray projection through the phantom.

#### 3.1 Breast phantoms of different cup size and percent density

To cover anatomical variations in breast size, we generated phantoms of different volumes by changing the simulation parameters. Based on the ranges of breast volume corresponding to different bra cup sizes, found in the literature<sup>27</sup>, we simulated five phantoms corresponding to cup sizes: A (volume=250ml), B (450ml), C (700ml), D (950ml), and DD (1500ml). Fig. 7 shows the central sagittal sections of the five phantoms with different cup sizes. The five phantoms were simulated assuming the same range of the adipose compartments size; as a result, the number of compartments in each phantom varied from 200 to 1050.

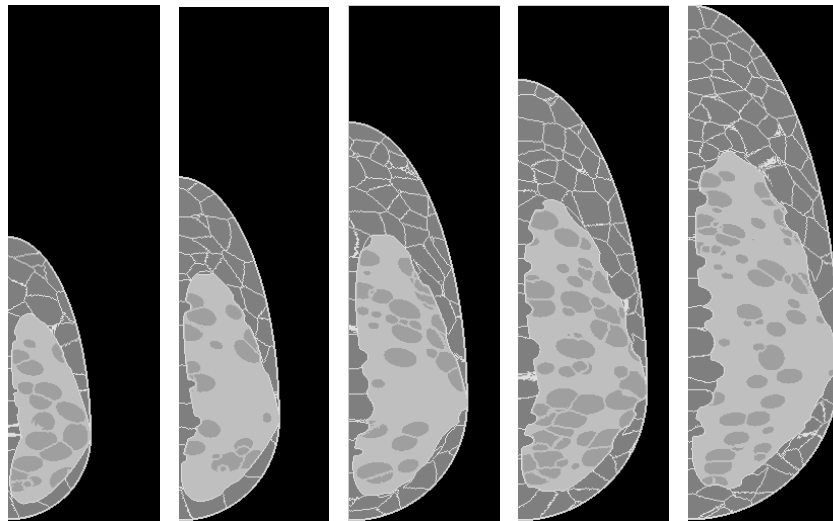


**Figure 7:** Sagittal sections through five realizations of the software breast phantom, corresponding to bra cup sizes (left to right) of A, B, C, D and DD. The number of adipose compartments was 200, 330, 500, 710 and 1050.

The five phantoms shown in Fig. 7 were generated with similar PD values ( $PD=38\pm3\%$ ). For a fixed cup size, the tissue PD is primarily determined by the size of the predominantly large scale FGT region. An accurate glandular PD value can be obtained by modifying the stopping criteria of the region growing simulation inside the FGT region. Fig. 8 shows three different phantoms of cup size B with PD values of (left to right): 25%, 50%, and 75%.

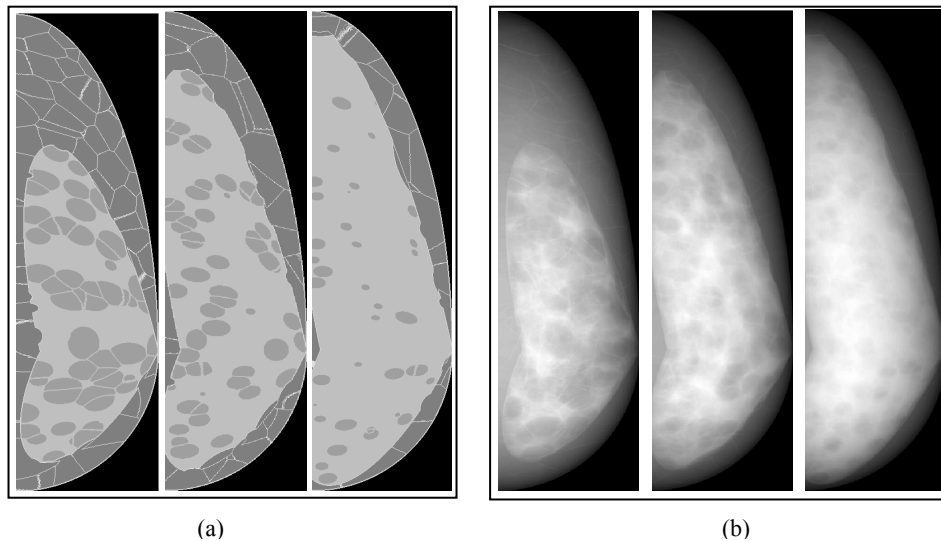


**Figure 8:** (a) Central sagittal sections of three phantoms generated with PD values of 25% (left), 50% (center), and 75% (right).. (b) Simulated X-ray projections through the phantoms from (a).

### 3.2 Breast phantoms of different compartment sizes

Software phantoms generated with different sizes of the adipose compartments are illustrated in Fig. 9. Three phantom realizations were generated using (left to right): 80, 200, and 400 seeds in the AT region, and 50, 150, and 300 seeds in the FGT region. The corresponding PD values are equal to 31%, 38% and 37%. The average volumes of the adipose compartments in the AT (FGT) region are  $3.22 \text{ cm}^3$  ( $2.19 \text{ cm}^3$ ),  $1.30 \text{ cm}^3$  ( $0.57 \text{ cm}^3$ ) and  $0.66 \text{ cm}^3$  ( $0.34 \text{ cm}^3$ ), for the three phantom realizations (from left to right) in Fig. 9(a). The histograms of compartment volumes for the three phantom realizations are shown in Fig. 10.

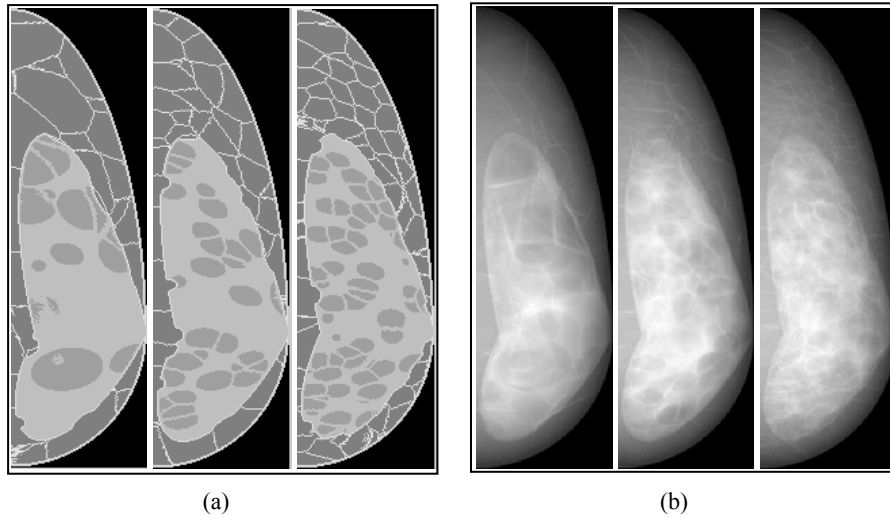


**Figure 9:** (a) Central sections of three phantom realizations with different ranges of compartment size. (b) Simulated X-ray projections through the phantoms from (a).

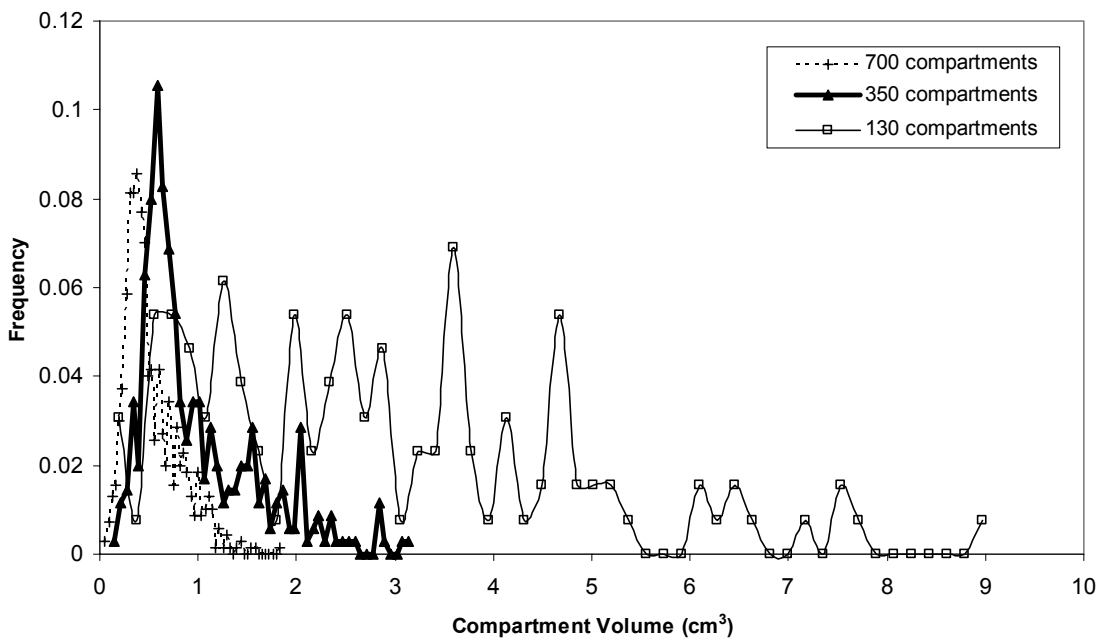


**Figure 10:** Comparison of histograms for the three phantom realizations with 130, 350 and 700 adipose compartments.

### 3.3 Breast phantoms of different thickness of compartment walls

Fig. 11 shows sections and simulated projections through the phantoms generated with compartment walls thickness of (left to right): 1 voxel, 3 voxels, and a mixture in which 50% of compartments are 1 voxel thick and 50% with 3 voxels thick.

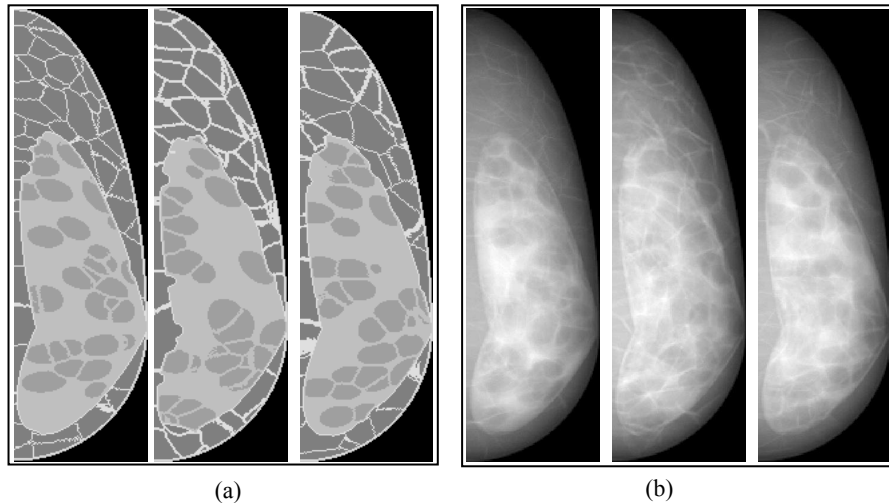


**Figure 11:** Central sagittal sections of three phantoms generated with compartment walls thickness of (left to right): 1 voxel, 3 voxels, and mixture of 50% of compartments with 1 voxel and 50% with 3 voxels thick compartment walls. (b) Simulated X-ray projections through the phantoms from (a).

#### 4. DISCUSSION

The proposed breast modeling method is capable of simulating breast phantoms of different cup size, glandularity and distribution of adipose compartments. The phantom cup size is determined by the volume of breast as parameterized by the ellipsoidal approximation of the breast outline. The phantom PD is determined by the size of the FGT region and the size of FGT adipose compartments. The distribution of adipose compartments is determined by the parameters of the region growing procedure. The number of adipose compartments determines the average compartment size; for a fixed cup size, the more compartments included, the smaller the average compartment size. The variation in compartment volumes depends on the compartment growth rates; the larger the range of growth rates, the larger the variation in compartment volumes. The final shape of the compartments depends on their initial distribution, orientations and growth rates.

The region growing approach could be further expanded to include more control over the region number, shape, and growing speed. We are working to include the ductal tree, pectoral muscle and small scale anatomical details to our breast phantom. Further improvement of the phantom requires collection of more anatomical data from histologic slides and clinical images with improved acquisition parameters to allow for more accurate estimation of phantom parameters.

#### 5. CONCLUSIONS

We have proposed a realistic simulation of the breast anatomy and clinical images in the form of a software breast phantom. The software phantom represents an extension of our previous computer breast model. The matrix of adipose compartments and Cooper's ligaments is simulated using a region growing procedure. Two different stopping criteria were implemented to simulate different distribution of adipose compartments in the AT and FGT regions. Using the proposed modeling approach, we were able to simulate a wide range of phantoms with different cup size, tissue glandularity, or compartment size distribution.

#### ACKNOWLEDGMENT

This work was supported by Susan G. Komen Breast Cancer Foundation Research Grant BCTR133506, NIH Delaware Idea Networks of Biomedical Research Excellence (INBRE) Grant and NIH Grant NIH-R01-CA102758. The authors would like to thank Dr. S. J. Glick, University of Massachusetts, for providing the breast CT images of mastectomy specimen. The authors would also like to Dr. R.D. Cardiff, University of California, Davis, for providing the images of breast subgross histology specimens.

## References

1. Mammography, ACoQAI. *Mammography quality control manual*. Reston, VA: American College of Radiology. (1999).
2. Vedula, AA, Glick, SJ, Gong, X. "Computer simulation of CT mammography ". Paper presented at: SPIE Medical Imaging 5030. San Diego. 349-360. (2003).
3. Richard, FJP, Bakic, PR, Maidment, ADA. "Mammogram registration: a phantom-based evaluation of compressed breast thickness variation effects". *IEEE Transaction of Medical Imaging*. 25(2). 188-197. (2006).
4. Wagner, RF. "Lessons from my dinners with the giants of modern image science". *Radiat. Prot. Dosimetry*. 114(1-3). 4-10. (2005).
5. Hoeschen, C, Tischenko, O, Dance, DR, Hunt, RA, Bakic, PR, Maidment, ADA. "Testing a wavelet based noise reduction method using computer simulated mammograms". Paper presented at: SPIE Medical Imaging. San Diego, CA. 969-978. (2005).
6. Caldwell, CB, Yaffe, MJ. "Development of an anthropomorphic breast phantom". *Medical Physics*. 17(2). 273-280. (1990).
7. Bochud, FO, Abbey, CK, Eckstein, MP. "Statistical texture synthesis of mammographic images with clustered lumpy backgrounds". *Optics Express*. 4(1). (1999).
8. Heine, JJ, Deans, SR, Velthuisen, RP, Clarke, LP. "On the statistical nature of mammograms". *Medical Physics*. 26(11). 2254-2265. (1999).
9. Taylor, P, Owens, R. "Simulated Mammography using Synthetic 3D Breasts". Paper presented at: 4th International Workshop on Digital Mammography. Nejmegen, Netherlands. 283-290. (1998).
10. Bliznakova, K, Bliznakov, Z, Bravou, V, Kolitsi, Z, Pallikarakis, N. "A three-dimensional breast software phantom for mammography simulation". *Physics in Medicine & Biology*. 48(22). 3699-3719. (2003).
11. Bakic, PR, Albert, M, Brzakovic, D, Maidment, ADA. "Mammogram synthesis using a 3D simulation. I. Breast tissue model and image acquisition simulation". *Medical Physics*. 29(9). 2131-2139. (2002).
12. Bakic, PR, Brzakovic, D. "Simulation of digital mammogram acquisition". Paper presented at: SPIE Medical Imaging. San Diego, CA. 866-877. (1999).
13. Richard, FJP, Bakic, PR, Maidment, ADA. Non-rigid registration of mammograms obtained with variable breast compression: A phantom study. In: Gee JC, ed. *Biomedical Image Registration*. Vol LNCS 2717. Berlin, Germany: Springer-Verlag. 281-290. (2003).
14. Hunt, RA, Dance, DR, Bakic, PR, et al. "Calculation of the properties of digital mammograms using a computer simulation". *Radiation Protection Dosimetry*. 114. 395-398. (2005).
15. Bakic, PR, Albert, M, Brzakovic, D, Maidment, ADA. "Mammogram synthesis using a 3D simulation. II. Evaluation of synthetic mammogram texture". *Medical Physics*. 29(9). 2140-2151. (2002).
16. Wellings, SR. "Development of Human Breast Cancer". *Advances in Cancer Research*. (31). 287-314. (1980).
17. Cooper, A. *On the Anatomy of the Breast*. Vol 1-2. London: Longman. (1840).
18. Johns, PC, Yaffe, MJ. "X-ray characterisation of normal and neoplastic breast tissues". *Physics in Medicine & Biology*. 32(6). 675-695. (1987).
19. Glick, SJ, Thacker, S, Gong, X, Liu, B. "Evaluating the impact of x-ray spectral shape on image quality in flat-panel CT breast imaging". *Medical Physics*. 34(1). 5-24. (2007).
20. Bakic, PR, Albert, M, Brzakovic, D, Maidment, ADA. "Mammogram synthesis using a three-dimensional simulation. III. Modeling and evaluation of the breast ductal network". *Medical Physics*. 30(7). 1914-1925. (2003).
21. Martin, LJ, Boyd, NF. "Potential mechanisms of breast cancer risk associated with mamographic density: hypotheses based on epidemiological evidence". *Breast Cancer Research*. 10(1). (2008).
22. Beare, R. "Regularized seeded region growing". Paper presented at: ISSM2002. Sydney, Australia. 91-99. (2002).
23. Gonzalez, RC, Wintz, PA. *Digital image processing*. 2nd ed ed: Addison-Wesley. (1987).
24. Serra, J. *Image Analysis and Mathematical Morphology*. London, U.K.: Academic Press. (1982).
25. Hammerstein, GR, Miller, DW, White, DR. "Absorbed Radiation dose in Mammography". *radiology*. 130. 485-491. (1979).
26. Ruitter, NV, Zhang, C, Bakic, PR, Carton, A-K, Kuo, J, Maidment, A. "Simulation of tomosynthesis images based on an anthropomorphic breast tissue software phantom". Paper presented at: SPIE Medical Imaging San Diego. (2008).
27. Ringberg, A, Bageman, E, Rose, C, Ingvar, C, Jernstrom, H. "Of cup and bra size: reply to a prospective study of breast size and premenopausal breast cancer incidence". *Int. J. Cancer*. 119(9). 2242-2243. (2006).